Lasers in Surgery and Medicine 25:304–314 (1999)

Simplified Treatment Planning for Interstitial Laser Thermotherapy by Disregarding Light Transport: A Numerical Study

Johan Olsrud, PhD,[1]* Ronnie Wirestam, PhD,[1] Bertil R.R. Persson, PhD,[1] and Karl-G. Tranberg, MD, PhD[2]

[1]Department of Radiation Physics, Lund University Hospital, SE-221 85 Lund, Sweden
[2]Department of Surgery, Lund University Hospital, SE-221 85 Lund, Sweden

Background and Objective: **The objective was to investigate the effect of light transport on the temperature distribution and the coagulated volume under conditions relevant to interstitial laser thermotherapy (ILT) of tumors in the human liver.**
Study Design/Materials and Methods: **Temperature distributions and coagulated volumes produced with a diffusing laser fiber or a conductive heat source, at equal output power, were numerically calculated for tissue with different optical penetration depths. Four irradiation times (5, 10, 20, and 30 min) were studied. A three-dimensional finite-element model was used to calculate the temperature distribution during heating with four conductive heat sources (no light emission). Results were compared with measured temperature distributions during laser irradiation in a gel phantom with known optical properties.**
Results: **Numerical calculations showed that the influence of light transport on the coagulated volume was negligible in tissue with optical penetration depths below 3–4 mm at all studied irradiation times. The phantom experiment indicated good agreement with the calculated temperature distribution, both with a single diffusing laser fiber and with four fibers.**
Conclusion: **Light transport influences coagulated volumes only slightly under conditions presented in this work, which is relevant to ILT of tumors in the human liver. Lasers Surg. Med. 25:304–314, 1999.**

Key words: coagulated volume; finite element method; MRI; optical penetration depth; temperature

INTRODUCTION

Interstitial laser thermotherapy (ILT) is a method for local destruction of malignant tumors in the liver [1–5], pancreas, breast, and brain [6–8]. Laser-induced coagulation is also a promising technique for treatment of benign prostatic hyperplasia [9–11] and menorrhagia [12].

Treatment of liver tumors may be performed percutaneously [3] and at laparotomy [2,5]. The

Grant sponsor: Swedish Cancer Society; Grant sponsor: Royal Physiographic Society in Lund; Grant sponsor: Lund Health Care District's Research Foundations; Grant sponsor: John and Augusta Persson's Foundation for Scientific Medical Research; Grant sponsor: Gunnar, Arvid and Elisabeth Nilsson's Foundation for Cancer Treatment.

*Correspondence to: Johan Olsrud, PhD, Department of Radiation Physics, Lund University Hospital, SE-221 85 Lund, Sweden. E-mail: johan.olsrud@mse.dll.se

Accepted 8 June 1999

blood flow may be occluded, which increases lesion volumes significantly [13–15]. Diffusing fibers allow heating of clinically relevant volumes, without carbonization, in a single irradiation session [16,17]. When the target volume is too large for treatment with a single fiber or when an irregular volume has to be treated, multiple fiber systems may be used for a single session treatment [18,19]. Fairly cheap and compact diode lasers further facilitate this technique. These developments have been important in trying to establish ILT as a method for local tumor treatment. What remains is further development of methods for planning, control and verification of the treatment effect. Mathematical models and noninvasive imaging modalities are being developed for these purposes [20,21]. Numerical calculations based on Monte Carlo simulation of the light transport, and subsequent finite difference modeling of the heat transport provide accurate estimations of the temperature distributions in vitro [20,22,23]. Mathematical modeling has also been validated in vivo [24], and good agreement between calculated lesion dimensions and corresponding dimensions determined by means of magnetic resonance imaging (MRI) has been reported [21]. Light transport influences the temperature distribution to a large extent close to the laser fiber, and the effects of optical and thermal diffusion has been studied theoretically for a point optical source by Wyman and Whelan [25]. At some distance away from the fiber, the photon irradiance is small, and the temperature distribution depends mainly on the thermal properties of the tissue and on blood perfusion. If the irreversibly damaged tissue volume extends beyond this distance, there is a possibility that the light distribution may be neglected in thermal treatment planning. A prerequisite is that this does not influence the clinically relevant results in terms of treated volumes. A moderate influence of light transport on the coagulated volume was noted by Prapavat et al. [23], but further investigation is required to determine whether and under what circumstances this might be used in thermal treatment planning.

The purpose of this work was to investigate whether diffusing laser fibers can be approximated by conductive heat sources during conditions that are relevant to ILT of tumors in the human liver. The temperature distribution and coagulated volume produced with a diffusing laser fiber, as compared with a conductive heat source, were studied by means of numerical calculations. A three-dimensional finite-element model was then used to calculate the temperature distribution during heating with four cylindrical heat sources (no light emission). The results were compared with the measured temperature distribution during irradiation with diffusing laser fibers in a gel phantom with known optical properties.

MATERIALS AND METHODS

Numerical Calculations

Temperature distributions and coagulated volumes with a single diffusing or conductive applicator. To calculate accurately the entire temperature distribution during laser irradiation of tissue, both the photon transport and the heat transport must be modeled. For this purpose, a computer simulation program (LITCIT version 4.6b, Laser und Medizin Technologie, Berlin, Germany), of which the accuracy has previously been extensively verified in vitro [20,23], was used. The energy fluence rate, E_0 (W m^{-2}), is calculated by Monte Carlo simulation of the photon transport, based on optical interaction coefficients that have been obtained from double integrating sphere measurements by Roggan et al. [26]. The input optical parameters of the program were the absorption coefficient μ_a (mm^{-1}), the scattering coefficient μ_s (mm^{-1}), and the average cosine of scattering angle g (dimensionless), also called the anisotropy factor. From these, the effective penetration depth δ_{eff} (mm), which is useful to compare the degree of light penetration in different tissue types, can be calculated:

$$\delta_{eff} = \frac{1}{\sqrt{3\mu_a[\mu_a + (1 - g)\mu_s]}}. \quad (1)$$

The heat transport is simulated by means of the method of finite differences to obtain a numerical solution to the bioheat transfer equation [27]:

$$\rho c \frac{\partial T}{\partial t} = \nabla \cdot (\lambda \nabla T) + Q_s + Q_p \quad (2)$$

where t (seconds) is time, T (°K) is the temperature, ρ (kg m^{-3}) is the density, c (J kg^{-1} K^{-1}) is the specific heat, and λ (W m^{-1} K^{-1}) is the thermal conductivity of the tissue. The spatially distributed heat-source term Q_s (W m^{-3}), due to absorption of the laser light, is calculated as the product of the energy fluence rate and the absorption coefficient. The energy removal due to perfusion Q_p (W m^{-3}) was not considered in this article.

The geometry of the simulated volume with a

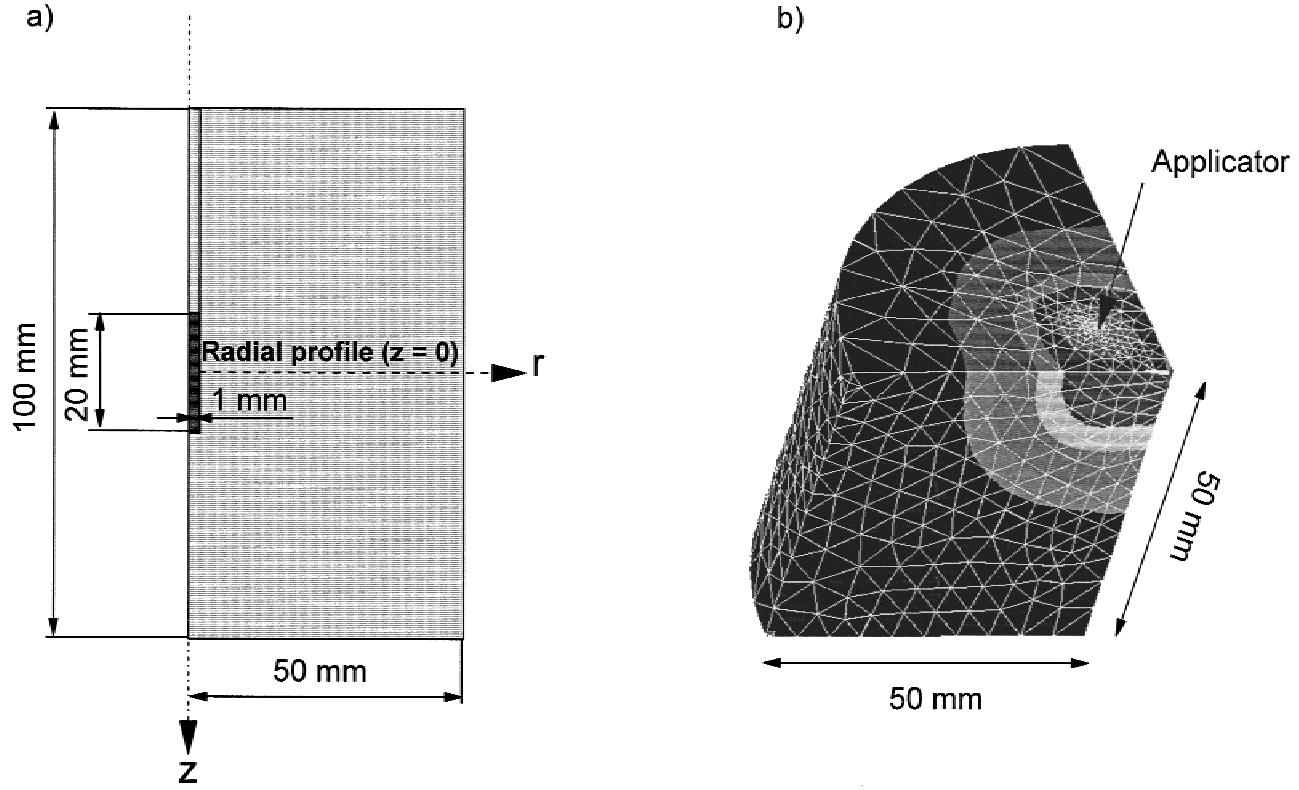

Fig. 1. Schematic illustration of **(a)** the axially symmetric model geometry in the single applicator simulations and (**b**) the three-dimensional finite-element model geometry used for simulation of four conductive applicators.

single interstitial applicator was axially symmetric with 50 mm radius and 100 mm height (Fig. 1a). A 20-mm-long cylinder with 1 mm radius, aligned with the symmetry axis, represented the interstitial applicator, which was either a diffuse light source or a conductive heat source. The cylinder representing the tissue was divided into ring elements with a quadratic cross section ($\Delta r = \Delta z = 0.5$ mm), and the time step used in the simulations was 0.25 sec. The light distribution was calculated for each time step by following 500 photons along their path through the tissue. When a conductive heat source was simulated, all the energy leaving the applicator was absorbed in the elements adjacent to the applicator surface. In all simulations, the outer boundaries were insulated.

Simulations of 5, 10, 20, and 30 min heating with either the diffusing fiber applicator or the conductive applicator were performed with optical properties corresponding to native and coagulated human liver at 850 nm and native human prostate at 1,064 nm. The thermal properties corresponded to native human liver, and the initial temperature of the simulated tissue volumes was 37°C. In addition, 30 min of laser irradiation of an optically tissuelike gel phantom was simulated to validate the model by comparison with experimental results. Prostatic tissue was included in the study because the optical penetration depth of this tissue has been found to be relatively large [26] and, therefore, may be expected to provide an upper limit of the errors that are introduced by disregarding light transport. The optical properties and the water contents used in the simulations are presented in Table 1. The water content was used to estimate the thermal properties [20]. For each tissue type and irradiation time, a constant power leaving the diffusing applicator was chosen to achieve a maximum temperature of 100 ± 2.5°C by the end of the irradiation. For the gel, the power was chosen to equal the actual power used in the experiment. The power used with the conductive applicator was always the same as the power used in the corresponding simulations with a diffusing applicator.

Tissue damage was quantified by means of a single parameter, Ω (dimensionless), which was

TABLE 1. Optical Properties and Water Contents of the Simulated Tissue Types and Phantom Materials*

	Human liver		Human prostate	Agarose	
	Native	Coagulated	(native)	I	II
Wavelength (nm)	850	850	1,064	805	805
μ_a (mm^{-1})	0.03	0.03	0.03	0.03	0.17
μ_s (mm^{-1})	20	53	8	7.7	18
g	0.95	0.94	0.95	0.9	0.9
δ_{eff} (mm)	3.3	1.9	5.1	3.7	1.0
Water content (%)	77[a]	77[a]	77[a]	100	100

*Optical tissue properties were adapted from Roggan et al. [26] and the optical properties of the agarose preparations were determined from previously reported data [33]. μ_a, absorption coefficient; μ_s, scattering coefficient; g, average cosine of the scattering angle (anisotropy factor); δ_{eff}, effective penetration depth.

[a]Adapted from Cooper and Trezek [42].

calculated as damage integral according to the Arrhenius formalism [28]:

$$\Omega(\mathbf{r}, \tau) = A\int_0^{\tau} \exp\left\{-\frac{\Delta E}{RT(\mathbf{r},t)}\right\}dt \qquad (3)$$

where Ω ($\mathbf{r}$, τ) is the logarithm of the ratio of the original concentration of native state tissue constituent to the remaining concentration after a time τ, at the spatial coordinate $\mathbf{r}$. A is a frequency factor (s^{-1}), ΔE is an activation energy barrier (J mol^{-1}), and R is the universal gas constant (8.31 J mol^{-1} K^{-1}). The rate parameters A and ΔE are tissue dependent, but rather sparse experimental data exist. In the present calculations, parameters obtained by Takata et al. [29] for porcine skin at temperatures higher than 50°C were used, i.e., $A = 9.4 \cdot 10^{104}$ s^{-1} and $\Delta E = 6.7 \cdot 10^5$ J mol^{-1}. To define the border of the coagulated volume, a value of $\Omega = 1.0$ was used [28,30], which corresponds to denaturation of 63% of the native state tissue constituent.

The temperature distribution and the value of the damage integral (Ω) by the end of each simulation were studied along a radial profile crossing the center of the applicator (Fig. 1a). The radial distance from the fiber center, at which the temperature increase obtained with the diffusing applicator and the conductive applicator differed by 5%, was determined for each tissue type and irradiation time. The influence of light absorption was considered negligible at radial distances beyond this limit.

Temperature distribution with four conductive applicators. To calculate the temperature distribution with four conductive applicators, a three-dimensional (3D) finite-element model (Fig. 1b) was implemented by use of a commercially available finite-element analysis program (ANSYS version 5.3, ANSYS Inc., Houston, PA). The applicators were modeled as four 20-mm-long cylinders with 1 mm radius, parallel to each other, forming a box with 20-mm sides. The surrounding material was modeled as a 100-mm-long cylinder with 50 mm radius and with thermal properties as follows: $\lambda = 0.6$ W m^{-1} K^{-1}, $c = 4180$ J kg^{-1} K^{-1}, and $\rho = 1000$ kg m^{-3}. The initial temperature of the surrounding material was 22.5°C, and the power emitted from each applicator was 1.7 W (13,530 W m^{-2} at the applicator surface), as in the experiment to be described later. For symmetry reasons, the model could be reduced to one-eighth of the entire volume (Fig. 1b). Meshing of this volume resulted in 9,690 nodes, belonging to 6,111 tetrahedral elements. The element side length was 1 mm at the applicator surface and increased gradually to 10 mm at the outer boundaries. A boundary condition stating zero heat flux was applied at all outer boundaries and symmetry surfaces. A transient analysis corresponding to 15 min of heating was performed, with an initial time step of 0.01 sec and a maximum time step of 100 sec by the end of the simulation.

Experimental Validation

To validate experimentally the numerical model used for the single-applicator calculations and the approximation of disregarding the light distribution, the temperature distribution during laser irradiation of optically tissuelike agarose gel phantoms was measured by means of temperature-sensitive MRI with the proton-resonance frequency-shift method [31–33]. With this method,

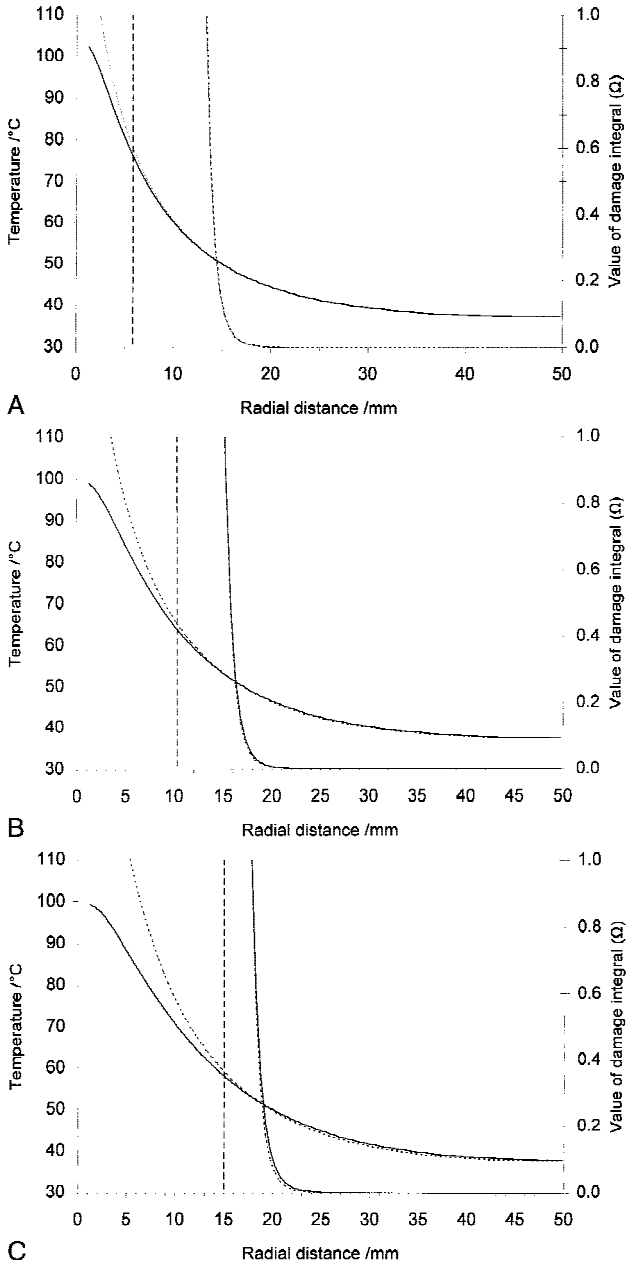

Fig. 2. Radial profiles (z = 0 in Fig. 1a) of the temperature and the damage integral with a diffusing laser fiber (—) or a conductive applicator (···) for **(A)** coagulated human liver, **(B)** native human liver, and **(C)** native human prostate after 30 min of heating. The largest shown value of the damage integral is 1.0, indicating the radial extent of the coagulated volume. The broken vertical lines indicate that the radial distances at which the temperature increase, with the two applicators, differs by 5%.

MR phase images are acquired and temperature change images are calculated by subtraction of a reference phase image, acquired before laser irradiation, from all other phase images. Using a standard gradient echo pulse sequence, temperature changes (ΔT) within each single volume element (voxel) can be calculated from the following equation [31]:

$$\Delta T = \frac{\Delta\varphi}{\gamma\, TE\alpha\, B_0} \quad (4)$$

where $\Delta\varphi$ is the measured phase angle change within the voxel after subtraction of the reference phase image, γ is the gyromagnetic ratio of hydrogen ($\gamma/2\pi = 42.577 \cdot 10^6\ s^{-1}\ T^{-1}$), and α is the proportionality constant in the linear temperature dependence of the proton resonance frequency [34]. B_0 represents the main magnetic field of the MRI scanner (1.5 T), and TE is the echo time of the gradient echo pulse sequence. All MR measurements were performed in a 1.5-T MRI scanner (Magnetom Vision, Siemens, Erlangen, Germany) using the standard head coil of the unit.

For irradiation with a single diffusing fiber (one experiment), a cylindrical phantom (height = 100 mm, radius = 40 mm) was prepared to approximate the optical properties of native human liver, with an effective penetration depth of 3–4 mm at 805 nm (Table 1). The absorption and scattering properties of the agarose gel phantom (agarose I in Table 1) were altered by addition of India ink (Higgins®, Eberhard Faber Inc., Lewisburg, TN) and latex microspheres (Mowilith 0530, Hoechst, Perstorp, Sweden). The dopant concentrations were determined from previously measured linear relationships between optical dopant concentrations and optical interaction coefficients at 805 nm: 0.08% ink and 0.8% (by weight) latex microspheres result in absorption and scattering coefficients of 0.03 mm^{-1} and 7.7 mm^{-1}, respectively [33]. The anisotropy factor (g) was previously measured to be approximately 0.9 at low ink concentrations [33]. To improve the signal-to-noise ratio, the T1 relaxation time of the gel was reduced by doping the solution with 5.3 mM Ni^{2+} [35]. Transmission through the laser fiber, with a 20-mm-long diffusing section and an outer diameter of 1.45 mm (Lightstic™, Rare Earth Medical, West Yarmouth, MA), was measured by using an integrating sphere power meter (Laser Therapeutics Inc., Buellton, CA). The fiber was molded into the phantom and connected to a diode laser (Diomed 25, Diomed, Cambridge, UK) emitting near infrared light with a 805-nm wavelength. Irradiation with a distal power of 3.2 W was then performed for 30 min, and MR images (TR/TE = 300/10 msec field of view [FOV] = 120 mm, flip angle [FA] = 68°, number of signal averages [NSA] = 1,

TABLE 2. Radial Distance at Which the Temperature Increase With a Diffusing Fiber and a Conductive Heat Source Differ by 5% ($r_{5\%}$), and the Radial Extent of the Coagulated Region ($r_{\Omega=1}$) for All Studied Tissue Types and Heating Times*

	Native prostate		Native liver		Coagulated liver	
Heating time/min	$r_{5\%}$/mm	$r_{\Omega=1}$/mm	$r_{5\%}$/mm	$r_{\Omega=1}$/mm	$r_{5\%}$/mm	$r_{\Omega=1}$/mm
5	10.5	10.8	8.0	9.2	5.6	7.9
10	12.3	13.2	9.2	11.2	5.9	9.9
20	13.7	15.9	10.1	13.6	5.9	11.9
30	15.1	18.9	10.3	15.2	5.9	13.4

*The resulting coagulated volumes are shown in Figure 3.

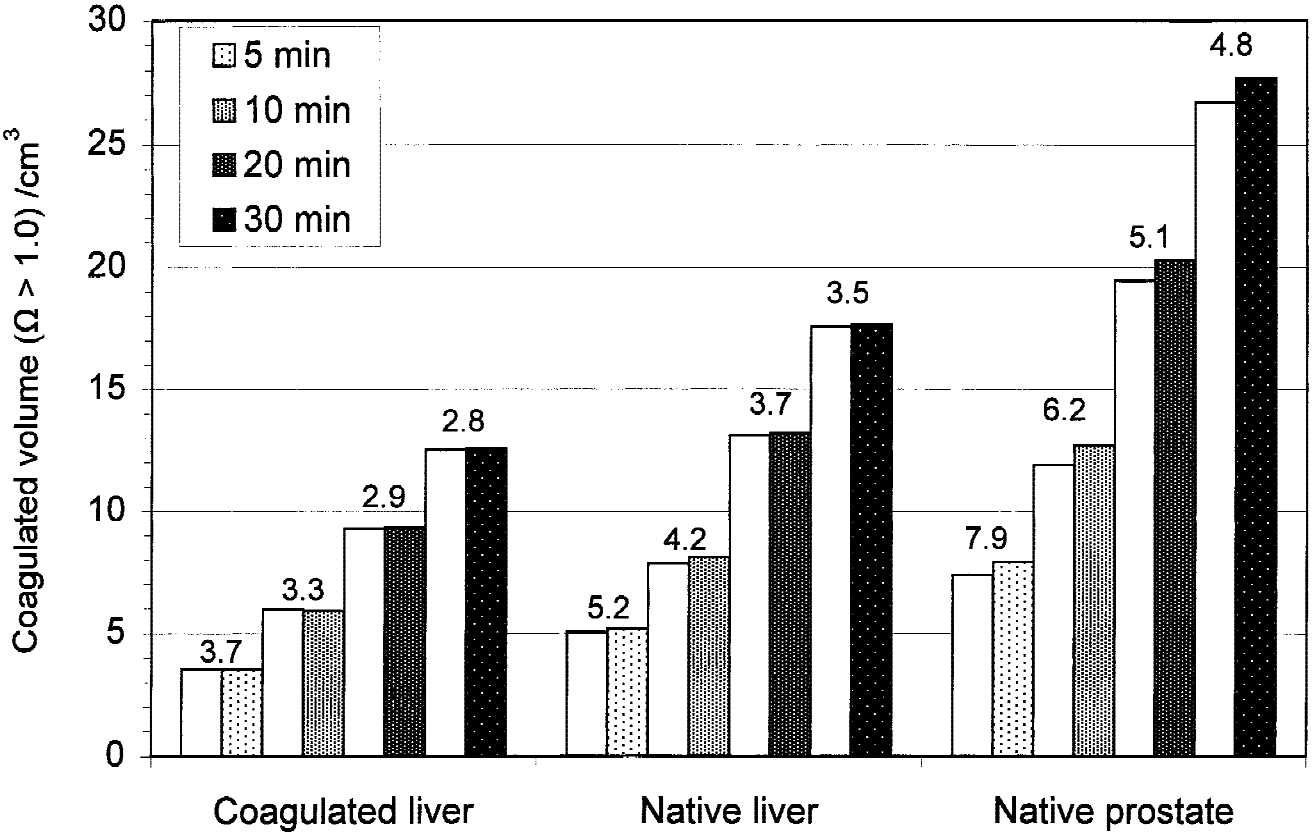

Fig. 3. Coagulated volumes after 5, 10, 20, and 30 min of simulated heating of tissue with different optical penetration depths. Volumes for a conductive applicator are illustrated by patterned bars, with blank bars to the left of them showing corresponding volumes with a diffusing laser fiber. Numbers above the bars are the constant power levels used in each simulation.

matrix size = 128^2, slice thickness = 5 mm, scan time = 40 sec) were acquired at 60 sec intervals from a transverse slice crossing the middle of the fiber. The temperature change image obtained after 30 min of irradiation was transferred to Matlab (MathWorks, Natrick, MA) for postprocessing. A radial temperature profile was determined by placing 1-mm-thick ring-shaped regions of interest (ROIs) at radial distances from the fiber axis ranging from 1.5 to 30 mm.

In the experiment (n = 1) with four diffusing fibers, the optical properties of the gel (agarose II in Table 1) were chosen to result in a small effective penetration depth at 805 nm. This will increase the chance that the simplification of disregarding light transport is valid, even quite close to the fibers, making it possible to get an indication of the accuracy of the finite-element model. The microsphere and ink concentrations were 2% and 0.4%, respectively, and resulted in absorp-

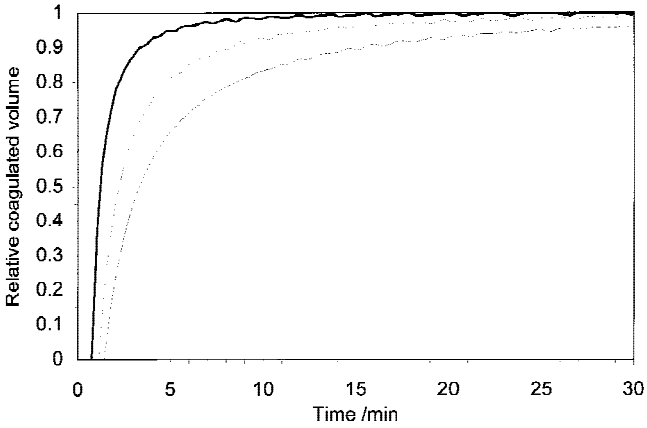

Fig. 4. Calculated ratio (relative coagulated volume) between coagulated volumes with a diffusing laser fiber and a conductive applicator as a function of time. Graphs show ratios with optical properties of coagulated human liver (—), native human liver (···), and native human prostate (—). Because of the discrete nature of the numerical calculations, graphs were smoothed by plotting the average ratio for each 30-second interval.

tion and scattering coefficients of 0.17 mm^{-1} and 18 mm^{-1}, respectively. The effective penetration depth in the phantom material, with an anisotropy factor of 0.9, was then 1.0 mm. Four laser fibers with 20-mm diffusing regions (Lightstic™, Rare Earth Medical) were connected to a beam splitter (Diomed), and the transmission through each fiber was measured. The laser light was found to be almost evenly distributed among the fibers, with relative transmissions ranging from 99% to 103%. The fibers were then molded into the gel phantom (55 mm radius and 90 mm height) parallel to each other, forming a square with 20-mm sides. Laser irradiation (mean distal power = 1.7 W/fiber) was performed for 15 min, and a transverse slice positioned through the middle of the diffusing sections of the fibers was used for MRI. Phase images were acquired each minute by use of a gradient echo pulse sequence (TR/TE = 300/20 ms, FA = 68°, FOV = 140 mm, NSA = 1, matrix size = 128^2, slice thickness = 5 mm, scan time = 40 sec). Actual temperatures were measured with a fluoroptic probe (Model 3000, Luxtron, Mountain View, CA) positioned within the imaging slice at the center of the square formed by the fibers. The temperature history at the position of the fluoroptic probe was evaluated by placing a circular ROI (0.5 cm^2) at the corresponding position in the temperature change images.

RESULTS AND DISCUSSION

Results from the simulations of interstitial heating with a diffusing laser fiber or a conductive applicator are shown in Figure 2A–C and in Table 2. The graphs show the results for tissue with optical properties corresponding to coagulated liver, native liver, and native prostate after a heating time representative for the procedure used at our department (30 min). The influence of light transport on the temperature distribution is illustrated by the radial temperature profiles. Close to the applicator surface, the temperature was overestimated when a diffusing laser fiber was approximated by a conductive applicator, but the discrepancy became smaller with increasing radial distances. In the same graphs, the value of the damage integral is shown, where $\Omega = 1.0$ is the largest value and indicates the radial extent of the coagulated volume. The radial distance at which the influence of light penetration on the temperature distribution was regarded as negligible (5% difference in temperature increase) was within the radial extent of the coagulated volume in all cases (Table 2). The difference between these two radial distances increased with increasing heating time and with decreasing optical penetration depth. In coagulated liver, the difference was 2–3 mm after 5 min of heating and increased to about 7 mm when the heating time was 30 min. For native liver and prostatic tissue with larger optical penetration depths, it was approximately 5 mm and 4 mm, respectively, after 30 min of heating. Thus, after 30 min of heating, the simplification of disregarding light transport was accurate to within 5% at a radial distance from the laser fiber, well within the extent of the coagulated volume, where the tissue can be assumed to be irreversibly damaged and the temperature distribution is less important. The radius of the coagulated (treated) volume increased with increasing heating time and was larger for tissue with larger optical penetration depth because of the higher heating power that could be used without exceeding a maximum temperature of 100°C. After 30 min of heating, the radius ranged from approximately 13 mm in coagulated liver to 19 mm in tissue with optical properties of native prostate (Table 2). It was also observed that the temperature profile with the conductive applicator crossed the profile with the diffusing applicator, leading to slightly underestimated temperatures at radial distances beyond the point of intersection. The ef-

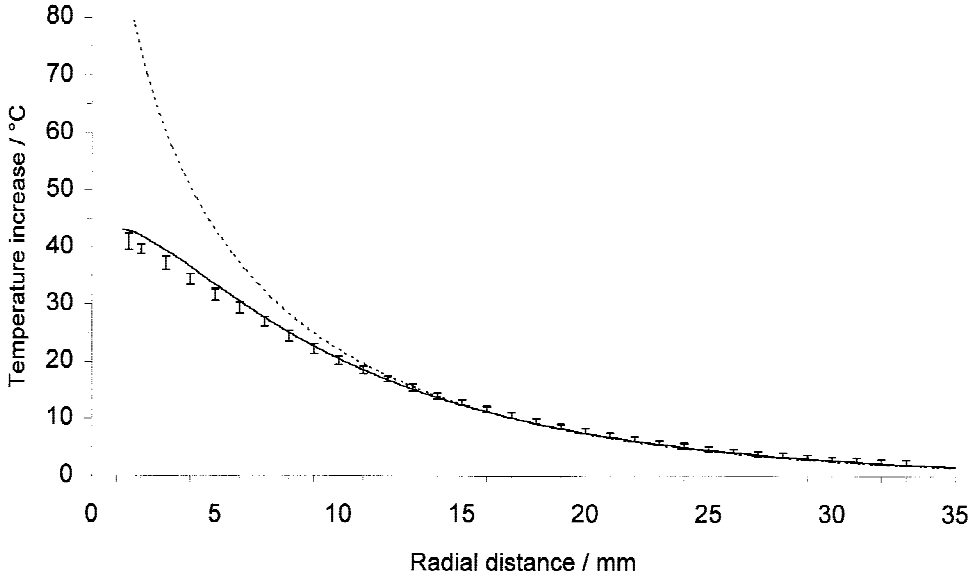

Fig. 5. Measured (I bars) and calculated (—) temperature-increase profile in optically doped agarose gel (agarose I) after 30 min of laser irradiation. The calculated profile for a conductive applicator (···) is also shown and aligns with the other profiles at a temperature increase of 15–20°C. The vertical bars correspond to ±1 SD, illustrating the precision of the magnetic resonance imaging temperature measurement.

fect was more pronounced for large optical penetration depths (Fig. 2C) and short irradiation times (not shown). Interestingly, the radius at which the curves crossed roughly corresponded to the estimated border of the coagulated volumes, leading to small errors at this clinically important region. The volumes of coagulated tissue ($\Omega \geq 1.0$) by the end of the simulations are illustrated in Figure 3, together with the heating power. With increasing optical penetration depth (coagulated liver having the smallest and native prostate the largest), the power that could be used without exceeding 100°C increased, with correspondingly larger coagulated volumes. Prolonged heating steadily led to larger coagulated volumes, even after times as long as 30 min because of the time dependence of the damage process (equation 2). For geometrical reasons, however, the radius grows more slowly with time as the coagulated volume increases. The estimated treated volumes with a diffusing laser fiber or a conductive applicator differed only slightly (<3%) when optical and thermal properties corresponding to coagulated liver or native liver were used in the model (Fig. 3). With the optical properties of prostate, the approximation of disregarding the light transport led to a slight overestimation of the coagulated volume. The time dependence is illustrated in Figure 4, where the ratio of the coagulated volumes ($V_{diff.\ appl.}/V_{cond.\ appl.}$) is plotted as a function of time for all studied tissue types and heating times. In agreement with a previous study [30], the coagulated volume was larger (ratio < 1) with a conductive applicator than with a diffusing applicator at the same power, especially at short heating times. The ratio asymptotically approached unity as the heating time increased; with a faster approach, for tissue with small optical penetration depth.

Experiments indicated that the numerical calculations rendered accurate results. The measured temperature increase along a radial profile after 30 min of irradiation in an optically tissue-like agarose gel (agarose I) is shown in Figure 5. In the same graph, the calculated temperature profiles for a diffusing laser fiber and a conductive applicator are shown. There was only a slight difference between the measured and calculated profiles for the diffusing fiber, most likely due to uncertainties in the optical properties of the gel. The calculated temperature profile for the conductive applicator differed from the measured profile close to the applicator, but they aligned at a distance from the applicator, where the temperature increase was 15–20°C, corresponding to a temperature of 52–57°C with a baseline temperature of 37°C. The measured two-dimensional temperature distribution after 15 min of irradiation with four diffusing fibers is shown in Figure 6 with the corresponding calculated temperature distribution with four conductive applicators. Calculated and measured temperature at an ROI (point A in Fig. 6) as a function of time is shown in Figure 7. Both MRI and fluoroptic probe measurements matched the calculated temperatures in this experiment.

Before ILT of liver tumors, it would be advantageous to be able to predict the optimal out-

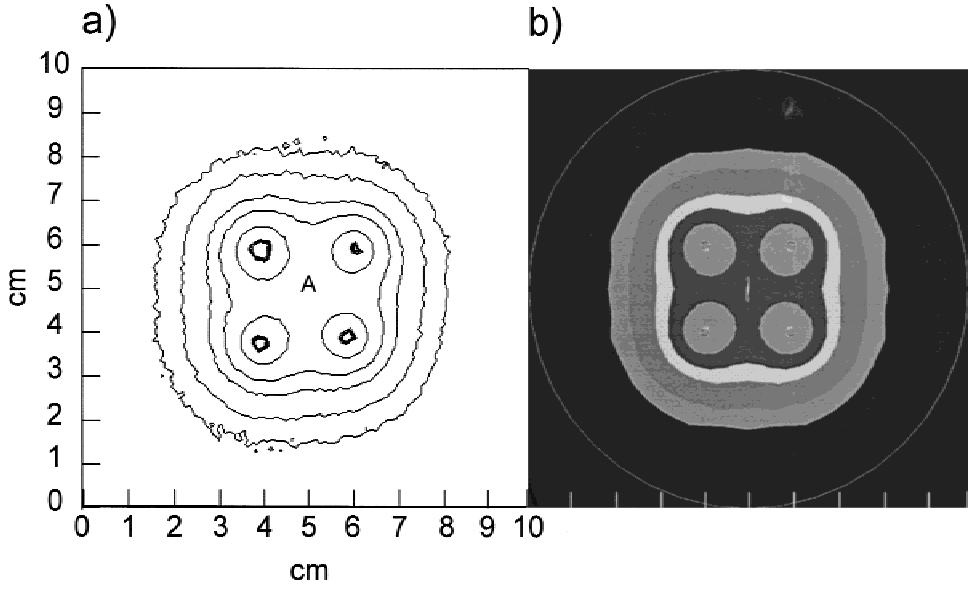

Fig. 6. **(a)** The two-dimensional temperature distribution with four diffusing fibers, as measured with magnetic resonance imaging, and **(b)** the FEM calculated temperature distribution with four conductive applicators. Contours correspond to 2.5, 5, 10, 15, and 25°C temperature increases.

put power and fiber placement. The maximum laser power that can be used, while the temperature at the surface of a single fiber stays slightly below 100°C, might be estimated from numerical calculations including both light and heat transport. However, it has been noted that the optical properties may not be very important to the extent of the coagulated volume [23]. In the present study, this observation was confirmed and further investigated with respect to the tissue type (optical penetration depth) and time. As illustrated by the quite similar coagulated volumes with a diffusing laser fiber and a conductive applicator, with optical and thermal properties corresponding to liver ($\delta_{eff} \lesssim 4$ mm), it appears to be possible to disregard light transport without miscalculating the treatment volume in this tissue. This finding could be used in clinical thermal treatment planning by omitting simulation of the light transport when the objective is only to predict the extent of the coagulated volume, and if the output power can be estimated beforehand. In support of this idea, the optical properties change as tissue coagulates, which generally leads to a substantial increase of the scattering coefficient, with a corresponding decrease in the effective penetration depth [36,37]. Therefore, after a few minutes of heating, the optical penetration depth in the region closest to the fiber will be less than 3 mm for most tissue, including liver metastases [26,38]. A consequence of the change in optical properties during coagulation is that the maximum power that can be used, while still avoiding evaporation and carbonization, is affected. Thus, an estimation of a suitable output power before a treatment could be quite difficult, especially because the optical properties also seem to differ significantly even within the same tissue type [37,38]. Germer et al. [38] investigated the optical properties in the near infrared range of normal liver and liver metastases before and after coagulation. They found a significant difference in optical penetration depth between liver metastases and normal liver, with a greater optical penetration depth in metastatic tissue. They also reported differences in the optical properties between different patients. In addition, the water content will be a parameter that could be subject to variations and that influences the maximum temperature. All these uncertainties might call for a modulation of the output power of the laser, so that a constant temperature, preferably just below 100°C, is maintained at the applicator surface [39,40]. Further study in vivo will be required to state wether an appropriate output power can be estimated, with a clinically acceptable uncertainty, before treatment.

The present calculations were performed and validated under in vitro conditions, without blood flow. However, the results should be valid in vivo during treatment of liver tumors when the blood flow is occluded [13,15]. For treatment of other organs, with uninterrupted blood flow, the situation is more complicated. Mathematical models used for treatment planning would then have to take temperature-dependent variations of the tissue perfusion and the influence of large blood vessels [41] into account. Additional concerns in vivo are the difficulty of accurately plac-

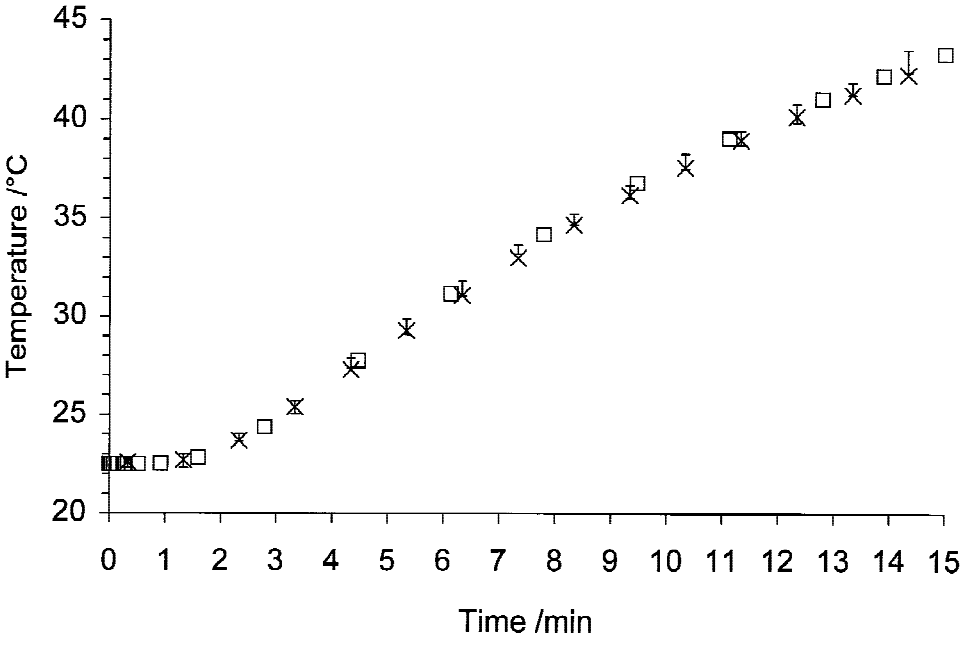

Fig. 7. Temperatures measured with magnetic resonance imaging (I bars) and a fluoroptic probe (×) during heating with four diffusing laser fibers, compared with Finite Element Method (FEM) calculated temperatures with four conductive applicators (□). Temperatures refer to point A in Figure 6, approximately 14 mm away from each fiber. The vertical bars correspond to ± 1 SD.

ing the fibers and the boundary conditions when tumors are located close to the surface of the liver. The finite-element method allows modeling of virtually any geometry, and may be a versatile treatment planning tool that allows the investigation of these effects. Furthermore, noninvasive temperature measurements in optically tissuelike phantoms may be used for such studies.

CONCLUSIONS

Numerical simulation of ILT treatment showed that, when blood flow is absent, the influence of light transport on the coagulated volume is small in tissue with optical properties similar to those of liver tissue and coagulated liver metastases. In tissue with a larger effective optical penetration depth, the coagulated volume tends to become somewhat overestimated when light transport is disregarded. It was also shown that the influence of light transport becomes less important to the treated volume as the heating time increases. Phantom experiments indicated good agreement with calculated temperature distributions, and the results are relevant for treatment of liver tumors when blood flow is occluded.

REFERENCES

1. Bown SG. Phototherapy of tumours. World J Surg 1983; 7:700–709.
2. Hashimoto D, Takami M, Idezuki Y. In-depth radiation therapy by YAG laser for malignant tumours in the liver under ultrasonic imaging. Gastroenterology 1985;88: A1663.
3. Masters A, Steger AC, Lees WR, Walmsley KM, Bown SG. Interstitial laser hyperthermia: a new approach for treating liver metastases. Br J Cancer 1992;66:518–522.
4. Amin Z, Donald JJ, Masters A, Kant R, Steger AC, Bown SG, Lees WR. Hepatic metastases: interstitial laser photocoagulation with real-time US monitoting and dynamic CT evaluation of treatment. Radiology 1993;187:339–347.
5. Tranberg K-G, Möller PH, Hannesson P, Stenram U. Interstitial laser treatment of malignant tumours: initial experience. Eur J Surg Oncol 1996;22:47–54.
6. Masters A, Bown SG. Interstitial laser hyperthermia in the treatment of tumours. Lasers Med Sci 1990;5:129–135.
7. Harries SA, Amin Z, Smith MEF, Lees WR, Cooke J, Cook MG, Scurr JH, Kissin MW, Bown SG. Interstitial laser photocoagulation as a treatment for breast cancer. Br J Surg 1994;81:1617–1619.
8. Kahn T, Bettag M, Ulrich F, Schwarzmaier H-J, Schober R, Fürst G, Mödder U. MRI-guided laser-induced interstitial thermotherapy of cerebral neoplasms. J Comput Assist Tomogr 1994;18:519–532.
9. McCullough DL, Roth RA, Babayan RK, Gordon JO, Reese JH, Crawford ED, Fuselier HA, Smith JA, Murchison RJ, Kaye KW. Transurethral ultrasound-guided laser-induced prostatectomy: National Human Cooperative Study results. J Urol 1993;150:1607–1611.
10. Norris JP, Norris DM, Lee RD, Rubenstein MA. Visual laser ablation of the prostate: clinical experience in 108 patients. J Urol 1993;150:1612–1614.
11. Cowles RS, Kabalin J, Childs S, Lepor H, Dixon C, Stein B, Zabbo A. A prospective randomized comparison of transurethral resection to visual laser ablation of the prostate for the treatment of benign prostatic hyperplasia. Urology 1995;46:155–160.
12. Garry R, Shelley-Jones D, Mooney P, Phillips G. Six hun-

dred endometrial laser ablations. Obstet Gynecol 1995; 85:24–29.
13. Möller PH, Hannesson PH, Ivarsson K, Olsrud J, Stenram U, Tranberg K-G. Interstitial laser thermotherapy in pig liver: effect of inflow occlusion on extent of necrosis and ultrasound image. Hepato-Gatroenterology 1997;44: 1302–1311.
14. Sturesson C, Liu DL, Stenram U, Andersson-Engels S. Hepatic inflow occlusion increases the efficacy of interstitial laser-induced thermotherapy in rat. J Surg Res 1997;71:67–72.
15. Heisterkamp J, van Hillegersberg R, Mulder PHG, Sinofsky EL, Ijzermans JNM. Importance of eliminating portal flow to produce large intrahepatic lesions with interstitial laser coagulation. Br J Surg 1997;84:1245–1248.
16. Panjehpour M, Overholt BF, Milligan AJ, Swaggerty MW, Wilkinson JE, Klebanow ER. Nd:YAG laser-induced interstitial hyperthermia using a long frosted contact probe. Lasers Surg Med 1990;10:16–24.
17. Heisterkamp J, van Hillegersberg R, Sinofsky E, IJzermans JNM. Heat-resistant cylindrical diffuser for interstitial laser coagulation: comparison with the bare-tip fiber in a porcine liver model. Lasers Surg Med 1997;20: 304–309.
18. Steger AC, Lees WR, Shorvon P, Walmsley K, Bown SG. Multiple-low-power interstitial laser hyperthermia: studies in the normal liver. Br J Surg 1992;79:139–145.
19. Ivarsson K, Olsrud J, Sturesson S, Möller P-H, Persson BRR, Tranberg K-G. Feedback interstitial diode laser (805 nm) thermotherapy system: ex vivo evaluation and mathematical modelling with one and four fibers. Lasers Surg Med 1998;22:86–96.
20. Roggan A, Müller G. Dosimetry and computer-based irradiation planning for laser-induced interstitial thermotherapy (LITT). In: Müller G, Roggan A, editors. Laser-induced interstitial thermotherapy. Washington: SPIE Optical Engineering Press; 1995. p 114–156.
21. Schwarzmaier H-J, Yaroslavsky IV, Yaroslavsky AN, Fiedler V, Ulrich F, Kahn T. Treatment planning for MRI-guided laser-induced interstitial thermotherapy of brain tumors—the role of blood perfusion. J Magn Reson Imaging 1998;8:121–127.
22. Sturesson C, Andersson-Engels S. A mathematical model for predicting the temperature distribution in laser-induced hyperthermia. Experimental evaluation and applications. Phys Med Biol 1995;40:2037–2052.
23. Prapavat V, Roggan A, Walter J, Beuthan J, Klingbeil U, Müller G. In vitro studies and computer simulations to assess the use of a diode laser (850 nm) for laser-induced thermotherapy (LITT). Lasers Surg Med 1996;18:22–33.
24. Beacco CM, Mordon SR, Brunetaud JM. Development and experimental in vivo validation of mathematical modeling of laser coagulation. Lasers Surg Med 1994;14: 362–373.
25. Wyman DR, Whelan WM. Basic optothermal diffusion theory for interstitial laser photocoagulation. Med Phys 1994;21:1651–1656.
26. Roggan A, Dörschel K, Minet O, Wolff D, Müller G. The optical properties of biological tissue in the near infrared wavelength range—review and measurements. In: Müller G, Roggan A, editors. Laser-induced interstitial thermotherapy. Washington: SPIE Optical Engineering Press; 1995. p 10–44.
27. Pennes HH. Analysis of tissue and arterial blood temperatures in the resting human forearm. J Appl Physiol 1948;1:93–122.
28. Henriques FC. Studies of thermal injury V: the predictability and significance of thermally induced rate processes leading to irreversible epidermal injury. Arch Pathol 1947;43:489–502.
29. Takata AN, Zaneveld L, Richter W. Laser induced thermal damage in skin. USAF School Aerospace Med, Brooks AFB, TX. Rep. SAM-TR-77-38; 1977.
30. Sturesson C. Interstitial laser thermotherapy: Influence of carbonization on lesion size. Lasers Surg Med 1998;22: 51–57.
31. De Poorter J, De Wagter C, De Deene Y, Thomsen C, Ståhlberg F, Achten E. The proton resonance frequency-shift method compared with molecular diffusion for quantitative measurement of two dimensional time dependent temperature distribution in phantom. J Magn Reson 1994;103:234–241.
32. Ishihara Y, Calderon A, Watanabe H, Okamoto K, Suzuki Yo, Kuroda K and Suzuki Yu. A precise and fast temperature mapping using water proton chemical shift. Magn Reson Med 1995;34:814–823.
33. Olsrud J, Wirestam R, Brockstedt S, Nilsson AMK, Tranberg K-G, Ståhlberg F, Persson BRR. MRI thermometry in phantoms by use of the proton resonance frequency shift method: application to interstitial laser thermotherapy. Phys Med Biol 1998;43:2597–2613.
34. Hindman JC. Proton resonance shift of water in the gas and liquid state. J Chem Phys 1966;44:4582–4592.
35. Morgan LO, Nolle AW. Proton spin relaxation in aqueous solutions of paramagnetic ions II Cr^{+++}, Mn^{++}, Ni^{++}, Cu^{++}, Gd^{+++}. J Chem Phys 1959;31:365–368.
36. Agah R, Gandjbakhche AH, Motamedi M, Nossal R, Bonner RF. Dynamics of temperature dependent optical properties of tissue: dependence on thermally induced alteration. IEEE Trans Biomed Eng 1996;43:839–846.
37. Nilsson AMK, Sturesson C, Liu DL, Andersson-Engels S. Changes in spectral shape of tissue optical properties in conjunction with laser-induced thermotherapy. Appl Opt 1998;37:1256–1267.
38. Germer C-T, Roggan A, Ritz JP, Isbert C, Albrecht D, Müller G, Buhr HJ. Optical properties of native and coagulated human liver tissue and liver metastases in the near infrared range. Lasers Surg Med 1998;23:194–203.
39. Glenn TN, Rastegar S, Jacques SL. Finite element analysis of temperature controlled coagulation in laser irradiated tissue. IEEE Trans Biomed Eng 1996;43:79–87.
40. Orth K, Duerr J, Hibst R, Steiner R, Beger HG. Thermocontrolled device for inducing deep coagulation in the liver with the Nd:YAG laser. Lasers Surg Med 1997;20: 149–156.
41. Whelan WM, Wyman DR, Wilson BC. Investigations of large vessel cooling during interstitial laser heating. Med Phys 1995;22:102–115.
42. Cooper TE, Trezek GJ. A probe technique for determining the thermal conductivity of tissue. J Heat Transfer Trans ASME 1972;94:133–140.